# Chapter 9

# A Protocol for Studying Transcription Factor Dynamics Using Fast Single-Particle Tracking and Spot-On Model-Based Analysis

**Asmita Jha and Anders S. Hansen**

## Abstract

Single-particle tracking (SPT) makes it possible to directly observe single protein diffusion dynamics in living cells over time. Thus, SPT has emerged as a powerful method to quantify the dynamics of nuclear proteins such as transcription factors (TFs). Here, we provide a protocol for conducting and analyzing SPT experiments with a focus on fast tracking ("fastSPT") of TFs in mammalian cells. First, we explore how to engineer and prepare cells for SPT experiments. Next, we examine how to optimize SPT experiments by imaging at low densities to minimize tracking errors and by using stroboscopic excitation to minimize motion-blur. Next, we discuss how to convert raw SPT data into single-particle trajectories. Finally, we illustrate how to analyze these trajectories using the kinetic modeling package Spot-On. We discuss how to use Spot-On to fit histograms of displacements and extract useful information such as the fraction of TFs that are bound and freely diffusing, and their associated diffusion coefficients.

**Key words** Single-particle tracking, Transcription factors, Live-cell imaging, Fluorescence microscopy, spaSPT, Spot-On, Diffusion, Single-particle trajectories, Single-molecule, Diffusion coefficient

## 1 Introduction

DNA-binding proteins such as transcription factors (TFs) play key roles in essentially all nuclear processes including gene regulation, DNA repair, and replication. TFs diffuse throughout the nucleus as they search for and bind their cognate DNA binding sites and recruit cofactors, chromatin remodelers, and general transcriptional machinery before dynamically dissociating from chromatin to begin a new cycle [1] (Fig. 1). Much of our current understanding of TFs has come from structural, biochemical, and genomics approaches. For example, structural methods such as cryo-EM have revealed how DNA-binding domains interact with DNA at atomic resolution, biochemical reconstitution approaches have revealed hierarchical and sequential binding of the general transcription

Julia Horsfield and Judith Marsman (eds.), *Chromatin: Methods and Protocols*,
Methods in Molecular Biology, vol. 2458, https://doi.org/10.1007/978-1-0716-2140-0_9,

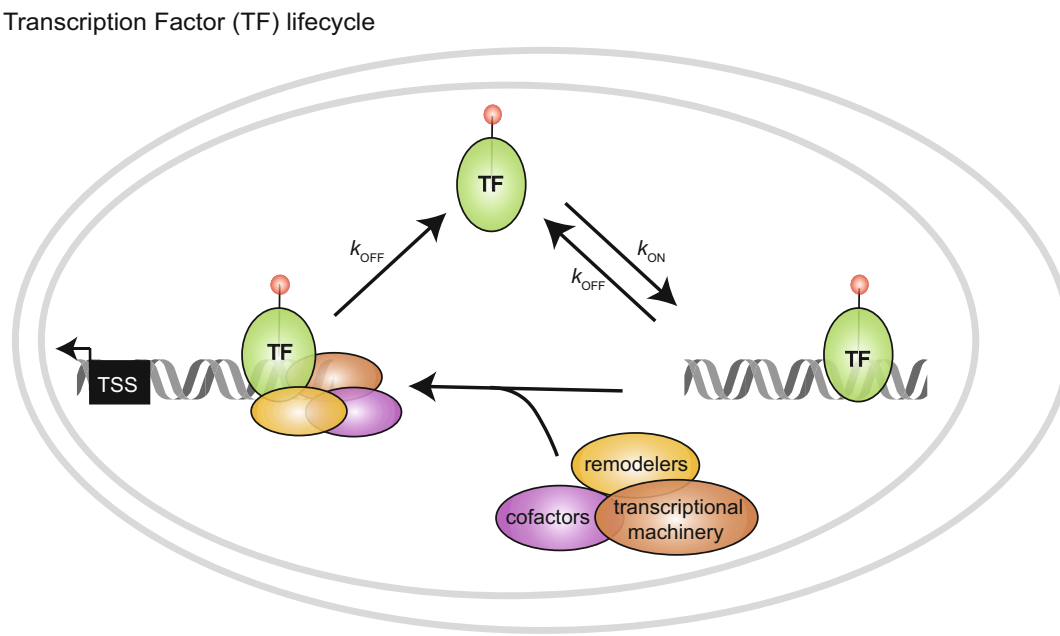


**Fig. 1** Outline of the dynamic life cycle of TFs. TFs undergo a dynamic life cycle inside the nucleus and can exist in multiple states. They diffuse, search for and bind to cognate DNA-binding sites, recruit cofactors and the general transcriptional machinery, and dissociate in search for the next DNA-binding site

factors, and genomic studies such as ChIP-Seq have shown where in the genome TFs bind [2]. However, many aspects of the dynamic TF life cycle inside living cells such as diffusion, target search mechanisms, DNA residence times, and clustering cannot be captured with these static, single snapshot approaches. Since understanding TF dynamics is essential for understanding TF regulation and function, live-cell imaging has thus emerged as a powerful tool to overcome these limitations and to track the real-time kinetics of a TF's dynamic life cycle.

Early work using live-cell imaging methods such as fluorescence recovery after photobleaching (FRAP) and fluorescence correlation spectroscopy (FCS) revealed DNA-binding of nuclear proteins to be highly dynamic [3–5]. In FRAP, a region of interest is photobleached and the rate of fluorescence recovery to the region of interest is subsequently observed. By monitoring how quickly bleached proteins exit the photobleached region and are replaced by unbleached proteins, dynamic protein parameters like diffusion coefficients and residence times can be estimated [6]. For example, a stably DNA-bound protein would be replaced at a slower rate and thus exhibit a slow FRAP recovery. FCS, on the other hand, measures the change in fluorescence in a small volume of interest. By analyzing the temporal correlation in fluorescence fluctuations and fitting kinetic models, one may infer diffusion coefficients, TF concentration, DNA binding and other parameters [7]. However,

because both FRAP and FCS probes bulk TF diffusion, target search, DNA binding, and DNA unbinding for many of TF molecules simultaneously, analysis of FRAP and FCS data requires complex reaction–diffusion modeling. Previous work and benchmarking approaches have demonstrated that conceptually distinct FRAP and FCS models sometimes fit experimental data equally well, which can make it challenging to quantitatively interpret FRAP and FCS data [5, 6, 8, 9].

Single-particle tracking (SPT) overcomes these limitations by enabling direct observation of individual fluorescently labelled proteins in single cells in real time [10]. In SPT, TFs are localized in each frame and then connected across frames to form trajectories. Through analysis of these SPT trajectories, we can then separate proteins into subpopulations based on their distinct diffusive behaviors, thus illuminating each aspect of the TF life cycle (Fig. 1) [1]. For example, since chromatin is a slow-moving scaffold, DNA binding of TFs can be observed as a change in the diffusion coefficient from a freely diffusing state ($D \sim 1$–$10\ \mu m^2/s$ for most TFs) to a slow-moving bound state ($D \sim 0.001$–$0.05\ \mu m^2/s$). Furthermore, by following the DNA-bound TFs over time, the residence time can be estimated [8, 11–13]. Once the bound fraction and residence time have been determined, the TF search time, how long a TF searches on average for a cognate site, can be calculated [14]. Moreover, anomalous diffusion and TF clustering can be inferred [15]. As such, SPT makes it possible to directly observe and quantify each aspect of the TF life cycle in living cells.

Recent applications of SPT have revealed how anomalous diffusion and transient trapping by protein clusters accelerate the TF target search mechanism [16] and suggested that longer TF residence times result in higher transcriptional output [17, 18]. Other SPT applications have focused on specific protein(s) such as the preinitiation complex assembly [19], TALEN and Cas9 nucleases [20], and the Polycomb proteins [21, 22]. Other SPT studies have quantified TF binding in in mitosis [23, 24] and how low-complexity domains affect TF dynamics [25]. Finally, SPT approaches have now matured to the point where single TF tracking inside living *Drosophila* and mouse embryos is possible [26].

At a high level, SPT methods applied to TFs and related proteins fall into at least three classes: "fastSPT," "slowSPT," and "all-in-one SPT." "fastSPT" approaches such as single particle tracking photoactivated localization microscopy (sptPALM) [27] and stroboscopic photoactivation SPT (spaSPT) [28] utilize imaging at high frame rates (~50–250 Hz) to track both bound and fast-diffusing TFs. Analysis of "fastSPT" data can reveal diffusion mechanisms, bound fractions, the number of diffusive states and more, but photobleaching rates are generally too high to infer residence times. Second, "slowSPT" uses long-exposure times to blur out fast-diffusing proteins and selectively focuses on slow-

diffusing, presumably chromatin-bound TFs [11, 29, 30]. Thus, slowSPT makes it possible to measure the residence time of the DNA-bound subpopulation, but cannot report on fast-diffusing subpopulations. "All-in-one SPT" approaches combine short exposures with variable dark times to attempt to simultaneously quantify the entire TF life-cycle including diffusion, number of states, and residence time [8, 12, 30, 31].

Here, we focus on "fastSPT," specifically spaSPT experiments. We will discuss how to optimize experimental and acquisition parameters, and how to analyze the resulting SPT data using Spot-On, a kinetic modeling framework that makes it possible to extract diffusion coefficients, the number of diffusive states, and the bound fraction from single-particle trajectories acquired from SPT experiments [28]. SPT experiments have four key steps: (1) cell preparation, (2) imaging, (3) trajectory generation, and (4) trajectory analysis (Fig. 2).

The first step of an SPT experiment is cell preparation. To be able to track single proteins, we must achieve sparse and bright fluorescent labeling. Typically, a TF is tagged as a genetically encoded fusion protein. Here, endogenous tagging using genome-editing is preferable, since it can avoid artifacts often associated with transient overexpression [14, 32]. Traditional fluorescent proteins such as GFP are not well-suited for SPT since SPT requires sparsity. Instead, photoswitchable proteins such as mEos and Dendra or self-labeling tags such as SNAP-Tag or HaloTag are preferred [27, 31]. HaloTag combined with bright organic dyes is the most popular approach since it combines superior photostability and brightness with high specificity and control over labeling density. Controlling labeling density is essential; if too few in-focus proteins are labeled, we obtain no trajectories, but if too many are

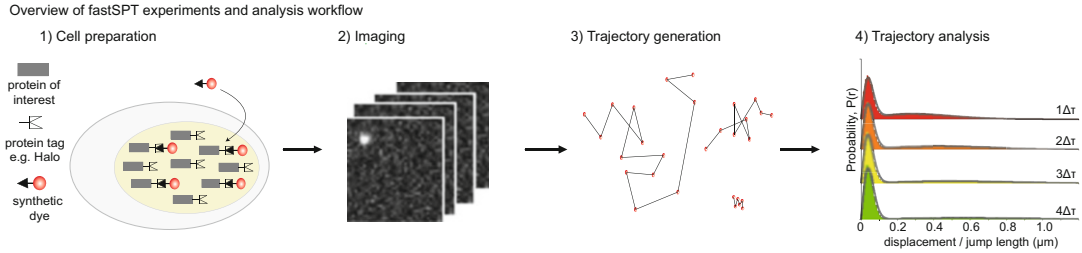


**Fig. 2** Overview of the key steps involved in conducting a "fastSPT" experiment and analyzing the data using Spot-On. A fastSPT experiments has four main steps. (1) Cell preparation: cells expressing a tagged protein of interest are labeled with a synthetic dye; (2) Imaging: fluorescence microscopy is then used to observe the movement of single labeled proteins (this figure was adapted from Video 2 from ref. 28 with permission). (3) Trajectory generation: particles are localized in each frame of the movies and tracked across frames to obtain SPT trajectories; (4) Trajectory analysis: SPT trajectories are analyzed using Spot-On to extract information about the diffusion coefficients and the bound and free subpopulations (shown: simulated SPT data with 50% bound and 50% free with $D_{FREE} = 4$ μm$^2$/s at 100 Hz)

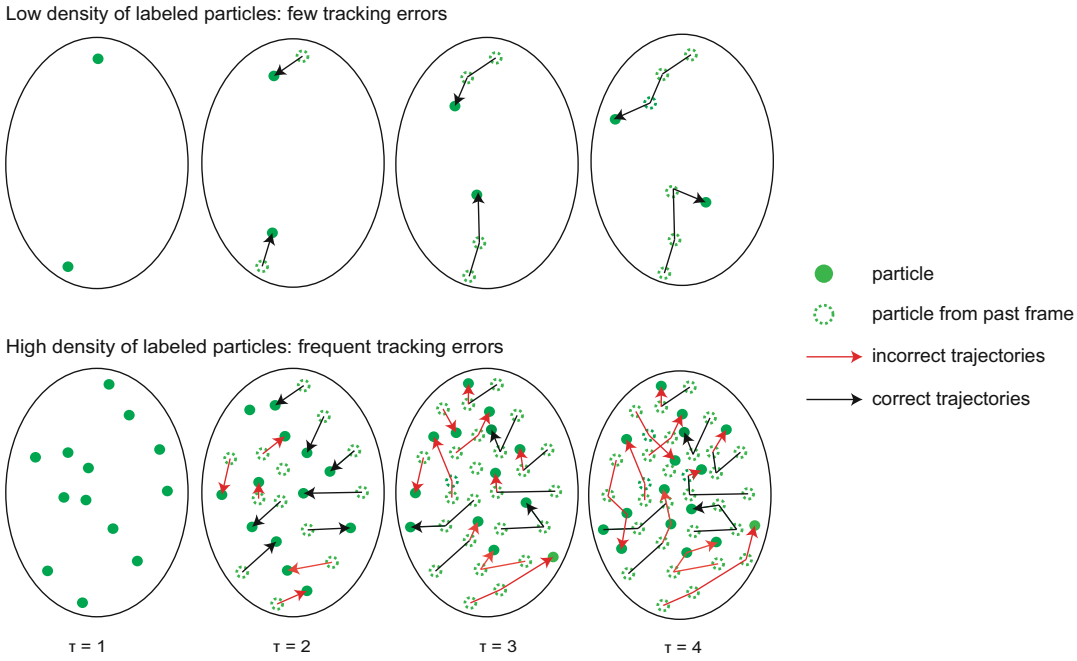


**Fig. 3** High particle densities result in frequent tracking errors (misconnections). Top panel: at low particle densities, particle trajectories can be clearly distinguished resulting in few misconnections. Bottom panel: at high particle densities, particle trajectories frequently overlap resulting in tracking errors (misconnections shown in red) when localizations are connected across frames during the tracking step

labeled, their paths will cross which leads to tracking errors (Fig. 3). Utilizing the HaloTag together with cell-permeable dyes such as Janelia Fluor (JF) dyes make it possible to control labeling density in two ways (Fig. 4) [33–35]. First, if "regular" JF dyes are used such as $JF_{549}$ or $JF_{646}$ [34], one can obtain a desired labeling density by titrating labeling time (typically 15–30 min) and dye concentration (typically ~1 pM to 5 nM depending on TF expression level). Second, one can control density using photoactivatable JF dyes, such as PA-$JF_{549}$ and PA-$JF_{646}$ [35] which only become fluorescent upon photoactivation using 405 nm illumination. With these dyes, one typically uses a higher labeling density (typically ~5 nM to 100 nM depending on TF expression level) to label many TFs and photoactivates a small fraction. The use of PA-dyes is recommended since it makes it possible to track TFs at very low densities such that tracking errors are minimized (Fig. 3) and facilitates simultaneous acquisition of thousands of trajectories by continuously photoactivating new subsets of TFs to compensate for photobleaching [27, 28]. With "regular" JF dyes one generally faces a hard trade-off between low density (few trajectories, few tracking errors) and high density (many trajectories, many tracking errors). However, PA-JF dyes are less cell-permeable, less chemically stable, and more prone to labeling artifacts especially

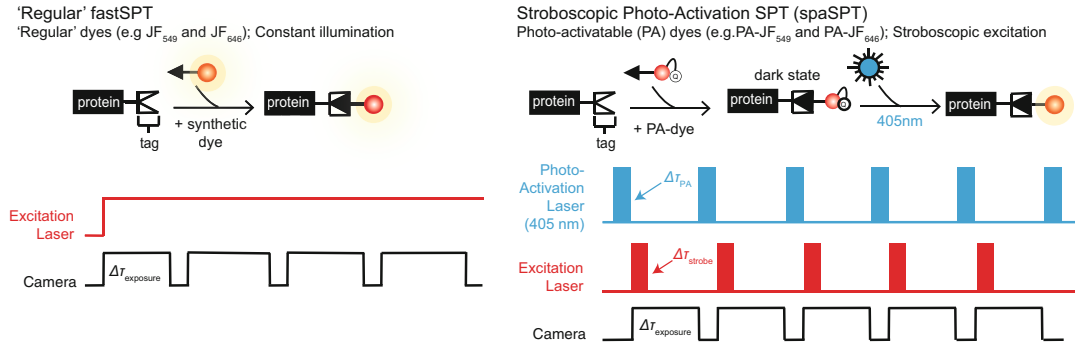


**Fig. 4** Overview and comparison of fastSPT with "regular" dye and spaSPT. Left: overview of "regular" fastSPT. Here, the protein of interest is labeled with a regular dye that is continuously fluorescent (e.g., $JF_{549}$ or $JF_{646}$) and excited with constant illumination from the excitation laser. Right: overview of stroboscopic photoactivation SPT (spaSPT). Here, the protein of interest is labeled with a photoactivatable (PA) dye that exists in a dark state, but which can be stochastically photoactivated into a fluorescent state using 405 nm illumination. This allows careful control of the density of fluorescent particles, and photoactivation of new proteins as existing ones photobleach which make it possible to obtain large numbers of trajectories, yet at low density. Stroboscopic pulsing of the excitation laser is used to minimize motion-blurring of fast-diffusing proteins and pulsing of the photoactivation laser during the camera read time is used to minimize background fluorescence

for low-to-moderately expressed proteins (unpublished observations). Thus, careful labeling control experiments should be performed if using PA-JF dyes.

Once cells expressing a tagged TF have been mounted on the microscope, we can proceed to the second step, imaging. In general, successful SPT acquisition requires a microscope with a high numerical aperture (NA) objective, a sensitive camera, and sufficiently powerful excitation lasers [9]. Most SPT studies use Highly Inclined and Laminated Optical Sheet (HILO) illumination since it conveniently reduces out-of-focus background fluorescence, thereby increasing the signal-to-noise ratio [36]. However, other modalities are also suitable for SPT, and a full discussion of suitable microscope modalities is beyond our scope. Here, we will focus specifically on how to optimize stroboscopic photoactivation SPT (spaSPT) imaging acquisition, though several considerations apply to SPT in general.

First, since chromatin-bound TFs are largely immobile, they produce a diffraction limited emission spot as expected from a point source, which can be precisely localized [37]. In contrast, detecting and localizing fast-diffusing TFs is challenging because as a frame is acquired, fast-diffusing TFs move and spread their emission photons across many pixels resulting in an imaging artifact known as *motion blur* (Fig. 5; [28, 38, 39]). For example, for a typical pixel size of 100 nm and TF $D = 3\ \mu m^2/s$, 53% of TFs would move at least 3 pixels during a $\Delta\tau = 10$ ms acquisition time (100 Hz) assuming

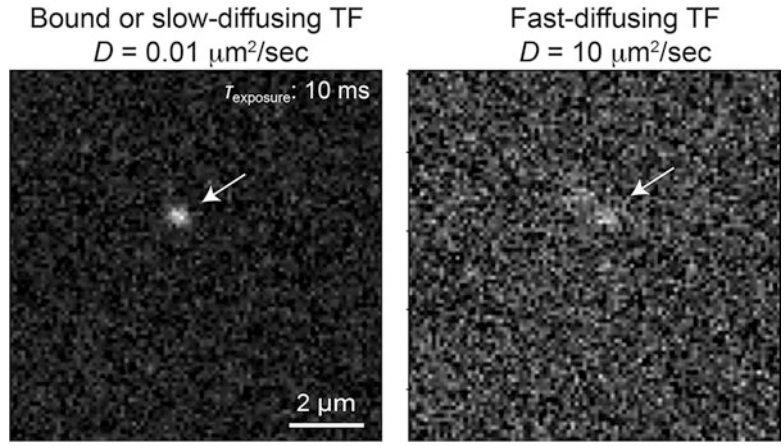


**Fig. 5** Illustration of motion-blurring of fast-diffusing particles. To illustrate the concept of motion-blurring, we simulated 2D Brownian motion with a timestep of 1 μs for a bound or slow-diffusing TF (Left: $D = 0.01$ μm$^2$/s) and for a fast-diffusing TF (Right: 10 μm$^2$/s) with a 10 ms exposure time with a pixel size of 110 nm. We used an Airy disc, following the Fraunhofer diffraction pattern for a circular aperture, as the point spread function and added realistic Poissonian photon shot noise, read noise, and dark current noise. Whereas bound and slow-diffusing particles are easily detected, detection and precise localization of motion-blurred fast-diffusing particles is extremely challenging which leads to bias

Brownian motion ($P(r > r_{\mathrm{MAX}}) = 1 - \exp\left(-r_{\mathrm{MAX}}^2/4D\Delta t\right)$). Since most localization algorithms assume diffraction limited emissions from an immobile point source [40], such motion blur can lead to both undercounting of the fast-diffusing subpopulation and imprecise localization [28, 41]. Stroboscopic excitation, whereby the excitation laser is pulsed, makes it possible to reduce motion blurring (Fig. 4). For example, using either a 2 ms or 1 ms excitation pulse, would reduce the fraction of TFs that move at least 3 pixels to 2.35% or 0.06%, respectively (100 nm pixels, $D = 3$ μm$^2$/s). Thus, stroboscopic excitation makes it possible to minimize motion blurring, though it requires sufficiently powerful excitation lasers to generate enough signal during the short exposure.

Second, photoactivation (405 nm) and excitation laser (e.g., 561 or 633 nm) powers should be optimized in spaSPT [28]. To minimize photobleaching, the excitation laser power should be set to the lowest power that gives sufficient signal-to-noise to reliably and precisely localize particles. To minimize tracking errors, but still obtain sufficient trajectories, a mean number of ~1–2 in-focus fluorescent particles per nucleus per frame is typically optimal. To achieve this, the 405 nm photoactivation laser power can be tuned: too high power will lead to too many activated fluorescent particles resulting in tracking errors; too low power, and there will be too few particles to track. If continuous photoactivation at low power is

used it will contribute background fluorescence. Pulsing the 405 nm photoactivation laser during the brief camera read time between frames conveniently avoids this (Fig. 4).

Third, we must optimize the frame rate. If the frame rate is too fast, TF displacements between frames will be difficult to distinguish from the localization uncertainty. If the frame rate is too slow, fast diffusing particles will defocalize (move out of the axial detection range of ±~350 nm) before we can track them. The average displacement, assuming 2D Brownian motion, between frames is given by $\sqrt{4D\tau}$. For a typical TF with $D \sim 3\ \mu m^2/s$, this translates to ~350 nm displacement for a frame rate of 100 Hz and ~250 nm displacements for a frame rate of 200 Hz which is substantially greater than typical 1D localization uncertainties of ~20–40 nm. Thus, for most TFs, frame rates of 100–200 Hz are optimal.

Once the movies have been acquired using optimized acquisition parameters we can proceed to the third step, trajectory generation [42]. Here we provide a brief discussion of trajectory generation; for an in-depth discussion please refer to [40, 42]. Trajectory generation consists of two steps: (1) localizing particles in each frame and (2) connecting the localized particles from frame to frame to form trajectories. First, sufficient signal-to-noise and low motion-blur is required for particle detection and precise particle localization [37, 42]. Localization involves first filtering and thresholding images to identify particles, followed by precise sub-pixel localization of the XY-coordinates. Most algorithms use point spread function (PSF) fitting to achieve this localization, though weighted centroid estimation is more robust to high motion-blurring [41]. Second, once the particles have been localized in each frame, they are connected across frames in the tracking step to generate trajectories (XY coordinates for each timepoint). Tracking algorithms vary from relatively simple like the nearest-neighbor and the Hungarian algorithms [43] to more complex such as the Multiple-Target Tracing [44] and u-track [45]. Some of these algorithms are conveniently available through ImageJ plugins such as TrackMate and the MOSAICsuite [43, 46]. Notably, if the SPT data is of high quality and the particle density is low (~<1–2 particles per frame), the choice of tracking algorithm plays a relatively minor role. For a tracking algorithm comparison, please *see* [40].

After single-particle trajectories have been generated, we can proceed to the fourth step, trajectory analysis. Here we focus on fastSPT analysis. One approach which we refer to as $MSD_i$ uses mean square displacement (MSD) analysis to estimate the diffusion coefficient of each trajectory, plots a histogram of diffusion coefficients ($Log(D)$), and then extracts subpopulations by fitting probability distributions to this histogram. Other methods attempt to estimate both the subpopulations and the transitions between them using Hidden Markov Modeling and/or Bayesian approaches [47–

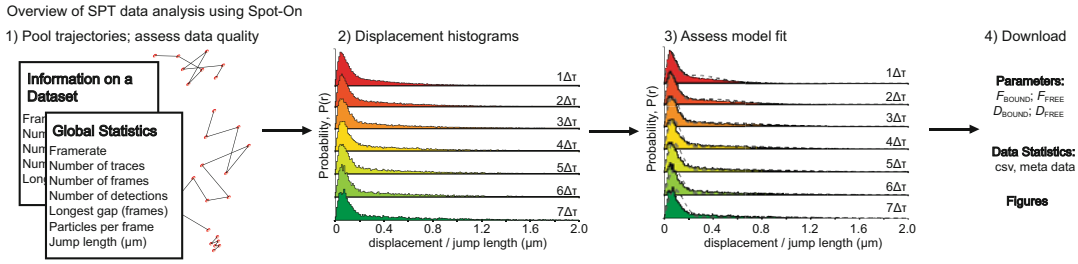


**Fig. 6** Steps involved in analyzing single-particle trajectories using Spot-On. Schematic of the Spot-On web-interface workflow: (1) upload single-cell datasets of pooled trajectories and assess global SPT data statistics; (2) generate histograms of displacements (jump lengths); (3) fit either a two-state or three-state model to the data and assess the fit; (4) download the fitted parameters

50]. However, these methods do not account for defocalization [51], which leads to an overestimation of the bound subpopulation, and in benchmarking studies $MSD_i$ approaches perform quite poorly [28]. These limitations can be overcome by pooling trajectories, fitting displacement histograms as a function of time, and then modeling defocalization as a function of the inferred diffusion coefficient of each subpopulation (Fig. 6). This approach was elegantly introduced by Mazza et al. in 2012 [8]. We subsequently simplified, expanded, and benchmarked this approach as Spot-On [14, 28]. Spot-On is available open-source in MATLAB and Python, as well as a convenient "no coding required" drag-and-drop web-interface, https://SpotOn.Berkeley.edu/.

The Spot-On web-interface is divided into three main sections (1) uploading single-particle trajectories, (2) generating histograms of displacements for multiple time points, and (3) fitting the displacement histograms to a kinetic model in order to estimate subpopulation sizes and their associated diffusion coefficients (Fig. 6). First, single-particle trajectories are uploaded to Spot-On and summary statistics are displayed (number of traces, their length, number of frames, etc.). Once the trajectories have been uploaded and assessed they can be used to generate a displacement histogram for multiple timepoints. After the displacement histogram has been generated, Spot-On proceeds to fit the histogram to a kinetic model using Brownian motion under steady state conditions without state transitions (i.e., it is assumed that transitions between the bound and free states are negligible in each individual trajectory). Spot-On offers fitting to two kinetic models: a two-state or a three-state model (Fig. 7). The two-state model considers a bound and free subpopulation and uses least-squares fitting to estimate three parameters: the bound fraction ($F_{\mathrm{BOUND}}$), the bound diffusion coefficient ($D_{\mathrm{BOUND}}$), and the free diffusion coefficient ($D_{\mathrm{FREE}}$); the free subpopulation is given by $1 - F_{\mathrm{BOUND}}$. The three-state model considers one bound and two free subpopulations and uses least-squares fitting to estimate five parameters:

the bound fraction ($F_{\mathrm{BOUND}}$), the bound diffusion coefficient ($D_{\mathrm{BOUND}}$), the slower free fraction ($F_{\mathrm{SLOW}}$), the slow free diffusion coefficient ($D_{\mathrm{SLOW}}$), and the faster free diffusion coefficient ($D_{\mathrm{FAST}}$); the faster free subpopulation is given by $1 - F_{\mathrm{BOUND}} - F_{\mathrm{SLOW}}$. A key advantage of Spot-On is that it accounts for defocalization due to 2D imaging of 3D motion [51], since axially diffusing particles will gradually exit the focal plane (±~350 nm). The rate of defocalization depends on the time interval between frames and the diffusion coefficient, leading to under-counting of the free subpopulations. Spot-On not only corrects for this bias, but the observed rate of defocalization, $Z_{\mathrm{corr}}$, is used as additional information to estimate the free diffusion coefficients with higher confidence [8, 14, 28] (Fig. 7). Spot-On can also optionally fit the 1D localization error, $\sigma$ (standard deviation of localization uncertainty). Finally, the user can download figures as well as the data and inferred parameters from Spot-On directly (Fig. 6).

We end by briefly discussing 2- vs. 3-state model selection and useful control SPT experiments. First, is a 2-state or 3-state model

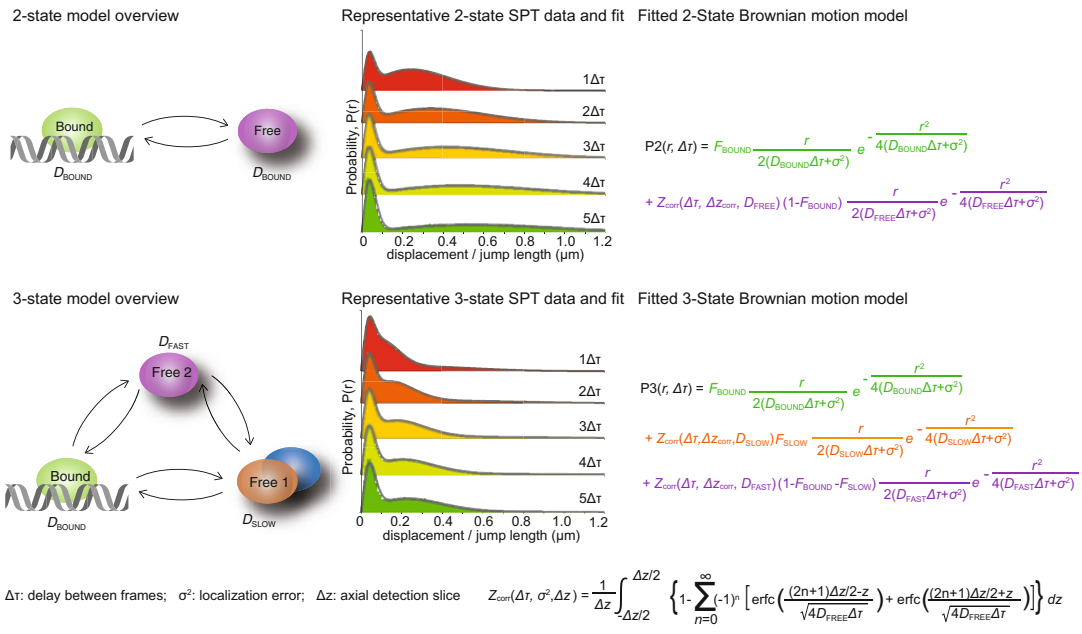


**Fig. 7** Overview of two-state and three-state models implemented in Spot-On. Top: The two-state model implemented in Spot-On models a chromatin-bound and free subpopulation while assuming Brownian motion. Representative data, fits, and the underlying model are shown. Middle: The three-state model implemented in Spot-On models a chromatin-bound and two free subpopulations corresponding to a slower and a faster free state while assuming Brownian motion. Bottom: Definitions and defocalization correction implemented in Spot-On. The datasets used to illustrate the models and fits were simulated using simSPT [28] with the following parameters for the 3-state model: $D_{\mathrm{BOUND}} = 0.01$ μm$^2$/s; $F_{\mathrm{BOUND}} = 0.25$; $D_{\mathrm{SLOW}} = 0.25$ μm$^2$/s; $F_{\mathrm{SLOW}} = 0.50$; $D_{\mathrm{FAST}} = 6.0$ μm$^2$/s; $F_{\mathrm{FAST}} = 0.25$; $\sigma = 25$ nm. To illustrate the 2-state model, the following parameters were used: $D_{\mathrm{BOUND}} = 0.01$ μm$^2$/s; $F_{\mathrm{BOUND}} = 0.2$; $D_{\mathrm{FREE}} = 3.0$ μm$^2$/s; $F_{\mathrm{FREE}} = 0.80$; $\sigma = 25$ nm

better? Given the higher number of free parameters, a 3-state model will always fit the data better. In particular, since diffusion inside the nucleus is generally non-Brownian and anomalous unlike the underlying Spot-On model, a slight mismatch between the data and a model fit is expected. Therefore, a slight mismatch between the data and 2-state model is not necessarily evidence for two freely diffusive states. We therefore generally favor the 2-state model unless the fit is quite poor or unless there are biological and mechanistic reasons to support the two free diffusive states in the three-state model. For example, components of the general transcriptional machinery such as Cyclin T1 and TBP can freely diffuse either as monomers or part of a larger multiprotein complex, thus motivating and justifying two distinct diffusive states in the three-state model [19, 52].

Finally, inclusion of controls is essential for validating SPT approaches. At a minimum, we suggest a "free" and "bound" control. An ideal "free" control is HaloTag fused to a nuclear localization signal (Halo-NLS). Halo-NLS should exhibit a minimal bound fraction (<15%) and exhibit a fast diffusion coefficient ($D \sim 8$–$12\ \mu m^2/s$); a substantially higher bound fraction or slower diffusion coefficient is a sign of too high motion blurring (note that the positively charged NLS affords some DNA binding to Halo-NLS [53]). Similarly, an ideal "bound" control is a stably bound protein such as a histone. Histone H2B (H2B-Halo) is a popular choice and should show a high bound fraction (>70%; some unbound H2B is expected if overexpressed from a non-cell cycle regulated promoter). Inclusion of Halo-NLS and H2B-Halo controls thus makes it possible to validate the "dynamic range" of TF behaviors that can be quantified. Furthermore, if a TF has a well-defined DNA-Binding Domain (DBD), we also suggest a ΔDBD-TF-Halo control.

In the following protocol, we discuss step-by-step how to conduct and analyze SPT experiments using mouse embryonic stem cells (mESCs) expressing an endogenous genetically encoded TF-Halo fusion protein as an example. This protocol can be modified depending on the cell line, protein of interest, fluorescent label, or microscope in use.

## 2 Materials

Below we described the required reagents and resources for the four main steps of a fastSPT experiment (1) reagents for cell preparation, (2) equipment for microscopy, (3) code for trajectory generation, and (4) analysis using Spot-On.

### 2.1 Reagents Needed for Cell Preparation

Cell preparation reagents are highly cell-type specific. Here we use reagents specific to mESCs that express a Halo-tagged TF as an example. All of the following reagents must be prepared in a biosafety cabinet, practicing strict sterile technique.

1. Growth Media: In order to prepare your growth medium, combine the following reagents: Knockout DMEM 1×, 15% Fetal Bovine Serum, 2 mM GlutaMAX Supplement, 1 mM MEM nonessential amino acids solution, 1000 U/mL LIF, 0.1 mM 2(β)-mercaptoethanol, 100 U/mL penicillin–streptomycin. Store at 4 °C.
2. Matrigel: dilute according to manufacturer's instructions prior to cell plating. Store aliquots at −20 °C. After being diluted in a serum-free medium, store at 4 °C (*see* **Note 1**).
3. Imaging dish: 35 mm dish, No. 1.5 Coverslip, 14 mm Glass Diameter, uncoated (*see* **Note 2**).
4. Trypsin-EDTA (0.05%), phenol red. Store at −20 °C.
5. Sterile 1× Phosphate Buffered Saline pH 7.4.
6. Biosafety Cabinet with Laminar Flow.
7. Tissue Culture (TC) incubator set to 37 °C and 5.5% $CO_2$.
8. Phenol-red free imaging Media: DMEM without phenol red, 15% fetal bovine serum, 2 mM GlutaMAX Supplement, 1 mM MEM nonessential amino acids solution, 1000 U/mL LIF, 0.1 mM 2(β)-ME, 100 U/mL penicillin–streptomycin. Store at 4 °C (*see* **Note 3**).
9. Dimethyl sulfoxide, sterile filtered.
10. Synthetic Dyes: Halo or SNAP dyes (e.g., PA-$JF_{646}$ or PA-$JF_{549}$). We recommend storing dyes at 1000× the desired concentration in DMSO at −20 °C in single-use aliquots to minimize freeze–thaw cycles [34, 35] (*see* **Note 4**).

### 2.2 Microscope Set-Up

Many microscope modalities are suitable for SPT, including wide-field microscopes. Here we use as our example a custom-built Nikon TI Microscope, implementing highly inclined illumination [36] that we previously used [14]. Key components include the following.

1. Live-cell incubation chamber heated to 37 °C that maintains a humidified atmosphere at 5.5% $CO_2$.
2. A high-NA objective. For HILO, we used a 100×/NA 1.49 Oil-immersion TIRF objective (Nikon apochromat CFI Apo TIRF 100× Oil).
3. Powerful excitation lasers matched to the desired fluorophores. We used 561 nm (1 W, Genesis, Coherent) for (PA)-$JF_{549}$; 633 nm (1 W, Genesis, Coherent) for (PA)-$JF_{646}$; 405 nm (140 mW, OBIS, Coherent) for photoactivation.

4. A fast and sensitive camera. Most EM-CCD and back-illuminated high quantum efficiency sCMOS cameras are suitable. We used an iXon Ultra 897 EM-CCD camera (Andor) (*see* **Note 5**).
5. Emission filters that match the fluorophores. We used: $JF_{549}$/PA-$JF_{549}$: Semrock 593/40 nm band-pass filter; $JF_{646}$/PA-$JF_{646}$: Semrock 676/37 nm bandpass filter.
6. Control of laser intensity. Rapid control (<100 μs) of laser intensity at multiple wavelengths is essential for stroboscopic excitation. We achieved this using an AOTF (AA Opto-Electronic, France, AOTFnC-VIS-TN) and DAQ card (National Instruments, NI-DAQ PCI-6723).
7. Microscope control software. We used Nikon Elements.

### 2.3 Localization and Tracking

Once raw SPT movies have been acquired, particles must be localized in each frame (localization) and then tracked between frames to form trajectories (tracking). Popular and user-friendly algorithms and implementations to achieve this include MTT [44], u-track [45], TrackMate [43], and the MOSAICsuite [46]. We used the MTT algorithm implemented in MATLAB (*see* **Note 6**). For a performance comparison of tracking algorithms, please *see* [40].

### 2.4 Analysis Using Spot-On

To analyze trajectory data using Spot-On, use either the web-interface, the MATLAB, or the Python version (*see* **Note 7**).

## 3 Methods

### 3.1 Cell Preparation

The following steps should be carried out in a biosafety cabinet and everything must be kept sterile. The steps apply to mESCs that express an endogenous genetically encoded TF-Halo fusion protein This protocol can be adjusted for the cell line, dye, or fluorophore in use.

1. Grow cells for seeding on tissue culture dishes until they are at 70–80% confluency.
2. Coat the glass bottom 35 mm imaging dish with Matrigel—Add 1 mL diluted Matrigel per imaging dish, spread and incubate at 37 °C and 5.5% $CO_2$ for 30–60 min (*see* **Note 8**).
3. Aspirate all of the media from the culture dish and wash cells with PBS. Gently swirl the PBS to ensure all residual media has been removed.
4. Aspirate PBS and add just enough 0.05% Trypsin-EDTA to cover the bottom of the culture dish and place in TC incubator for ~3 min.
5. Remove cells from the incubator and check if all the cells have thoroughly dissociated using a light microscope.

6. After cells have dissociated from culture dish, quench with normal culture medium, resuspend cells, pipet up and down with a P1000 pipette until all cell clumps have been broken up into single cells (*see* **Note 9**).
7. Transfer the desired number of cells to a 15 mL Falcon tube and centrifuge at 300 × *g* for 3 min. Enough cells should be used so that plated cells are ~70% confluent after overnight growth on the MatTek dish.
8. While cells are spinning down, remove Matrigel from **step 1** and add cell medium to the 35 mm imaging dish.
9. Remove tube from centrifuge and aspirate supernatant, leaving cell pellet.
10. Resuspend cell pellet in cell medium.
11. Add cells to the imaging dish at the appropriate density for the cell line in use. After adding cells to the imaging dish, gently swirl the dish to evenly distribute cells.
12. Place in TC incubator and grow overnight.

***Day of imaging*** After seeding imaging dishes the day before and verifying using a tissue culture microscope that they look healthy and are at ~70% confluency, we can proceed to dye labeling and imaging.

1. Prior to preparing cells for imaging, turn on the microscope and environmental chamber leaving enough time for the chamber to equilibrate to 37 °C and 5.5% $CO_2$ before imaging.
2. Prepare three 15 mL Falcons tubes: one with PBS; one with regular medium; and one with phenol red free Imaging Medium. Place these in the 37 °C water bath.
3. Remove the falcon with regular medium from the 37 °C water bath and make a dilution of the synthetic dye (e.g., Halo or SNAP compatible JF dye) to the desired concentration. Pipet up and down to mix (*see* **Note 10**).
4. Remove medium from the imaging dish and add medium with the desired concentration of synthetic dye and place in TC incubator for 15 min.
5. Wash 1: Remove Halo-dye medium and add prewarmed PBS, remove PBS, and add prewarmed medium and place in incubator for 5 min.
6. Wash 2: remove medium and add prewarmed PBS, remove PBS, and add prewarmed imaging medium without phenol red (more/longer washes may be necessary for PA-JF dyes) (*see* **Note 11**).
7. Cells are now ready to be imaged and can be stored in the TC incubator until the microscope is ready.

### 3.2 Imaging

The specific imaging protocol will be highly dependent on the microscope used, the desired SPT experiment, and a number of other factors. We briefly comment on some of the main steps below for fastSPT experiments.

1. Add immersion oil to the objective, then load the imaging dish with labeled cells on the prewarmed microscope.
2. Move the objective up until cells are in focus using either bright-field or fluorescence to focus on the cells.
3. If using HILO illumination, move stage to center the cell to be studied in the field-of-view. Modulate the TIRF angle until optimal HILO illumination is achieved (maximal signal-to-background ratio and even illumination of the whole nucleus).
4. If optimizing laser acquisition settings, then record a short movie (~500 frames) at the desired frame rate (typically ~100–200 Hz) changing only one parameter at a time. If using photoactivation, adjust 405 nm intensity and/or pulse duration until the desired density of particles is achieved (typically ~1–2 in-focus particles per nucleus per frame). If optimizing the main excitation laser (e.g., 561 nm for $JF_{549}$), record multiple short movies for different excitation powers and stroboscopic pulse durations, analyze the movies by generating trajectories, and overlay trajectories on raw movies. Choose an excitation setting that gives sufficient signal-to-noise that the localization algorithm misses almost no particles visible by eye in the raw images. Spending significant time iteratively optimizing acquisition settings is usually well worth the effort.
5. Once acquisition settings have been optimized, record fastSPT movies one cell at a time. After centering the field-of-view around a cell and optimizing the HILO angle (the optimal angle may need to be adjusted for each cell), crop a just big enough ROI around the nucleus of interest. Photobleach particles if necessary if the initial density is too high. Then record a fastSPT movie. Our default spaSPT acquisition parameters for most mammalian TFs are: 30,000 frames at 134 Hz, using 1 ms stroboscopic excitation (561 or 633 nm, 1 W, 100% AOTF power), and pulsing the photoactivation laser (405 nm, 140 mW, typically 1–4% AOTF) during the ~0.45 ms camera read-out time between frames.
6. Move at least two full field-of-views away and begin the next movie. We typically collect 6–8 movies per cell line per condition per day for at least three biological replicates performed on different days (at least 18–24 cells in total). Recording multiple cells is necessary to average over cell-to-cell and biological variation (e.g., cell cycle phase if cells are unsynchronized) and to obtain robust results.

7. Once finished with one cell line or condition, clean objective and mount a new imaging dish with a different cell line or condition.
8. Leave it at least 15 min to thermally equilibrate.
9. Then begin the next round of movies.
10. After imaging is complete, transfer all the raw SPT data, clean the objective, and turn off the microscope.

### 3.3 Trajectory Generation

Please *see* Subheading 2.3 for recommended localization and tracking algorithms. Below, we briefly outline the recommended steps after a day of SPT data acquisition.

1. Make sure to visually inspect SPT movies and visually assess the quality and reliability of the localization and tracking for a few movies by overlaying trajectories on the raw SPT movies.
2. Optimize localization and tracking algorithm parameters if necessary, but make sure to use consistent parameters for all conditions and replicates.
3. Once localization and tracking settings have been finalized, batch process all of the acquired SPT movies if possible.

### 3.4 Trajectory Analysis with Spot-On

Once trajectories have been generated, we can proceed to analysis. Here we specifically focus on how to analyze fastSPT data with Spot-On's web-interface. Please refer to the Spot-On paper [28] and the documentation available at https://SpotOn.berkeley.edu/SPTGUI/docs/latest for a more complete discussion.

1. Go to https://SpotOn.berkeley.edu/ and click "*Start spotting!*"
2. In "1. Select format" pick the format used for your SPT trajectories (*see* **Note 12**) and drag and drop your data into "3. Select datasets".
3. Make sure through "Uploaded datasets" that the files were successfully uploaded and assess "Global statistics" on the bottom right, which will display metadata for your uploaded SPT data (*see* **Note 13**).
4. Proceed to the "Kinetic Modeling" tab.
5. Under "Dataset selection" include all the datasets you would like to analyze. Click "all" if all the data are from the same condition.
6. Scroll down to "Jump length histograms" and inspect the histograms of displacements. Under "Display dataset" click through each cell to inspect that the data looks reasonable. Click "Show pooled jump length distribution" if you would like to combine the data from each single cell. Some noise is expected, but if the histograms are too sparse, the fitting is less likely to be accurate.

7. Scroll back up to "Parameters" and "Jump length distribution" and choose the desired values for "Bin width," "Number of timepoints," "Jumps to consider," "Use entire trajectories," and "Max jump" (*see* **Note 14** for a brief discussion of how to choose these parameters).
8. Next, proceed to "Model fitting." Choose between the two-state and three-state models, upper and lower bounds on the diffusion coefficients, whether to infer "Localization error" from the data (choose "fit from the data" or to predefine it (default is 35 nm or 0.035 μm)). Choose whether to use the *Z*-correction and if so, specify its value (default is 700 nm or 0.7 μm, which is reasonable for most high NA objectives). Finally, choose whether to use PDF or CDF fitting, whether to fit each single cell or only the merged displacement histogram of all of the cells, and the number of fitting iterations (*see* **Note 15** for a brief discussion of how to choose these).
9. Click "Fit kinetic model." This may take a few minutes.
10. If single-cell fitting was performed, scroll down to "display dataset" under "Jump length histograms" and scroll through each single cell and assess the quality of the fit and the cell-to-cell variation. This way any potentially problematic datasets can be identified (*see* **Note 16**). Once each single cell has been assessed, click "show pooled jump length distribution" to see the pooled data and fit.
11. Spot-On will display the fitted parameters for each single cell (if single cell fitting was chosen) and the global fit parameters: $D_{\mathrm{BOUND}}$, $D_{\mathrm{FREE}}$ ($D_{\mathrm{SLOW}}$, $D_{\mathrm{FAST}}$, if 3-state model), $F_{\mathrm{BOUND}}$, $F_{\mathrm{FREE}}$, ($F_{\mathrm{SLOW}}$, $F_{\mathrm{FAST}}$, if 3-state model), $\sigma$ (if localization error was fitted), and fitting parameter ($I_2$, AIC, BIC; *see* **Note 17**).
12. Iterate through the various options until a desired fit has been obtained.
13. Then scroll to the bottom of the page and click "Mark for download" and enter a name and description.
14. Next scroll back to the top of the page and click the "Download" tab. Here you can download individual figures (SVG, PDF, PNG, EPS) or you can click "Download all (zip)" to obtain a copy of the fitted parameters, raw data, as well as the figures.

## 4 Notes

1. When preparing Matrigel make sure everything is done on ice. Thaw individual aliquots on ice for 30 min prior to diluting in serum-free medium. Coating of glass with 0.1% gelatin is also appropriate, though in our experience adherence can be poorer.

2. A cover glass (e.g., Marienfeld-High-Precision 1.5H cover glasses, 0117650) mounted in an Attofluor Cell chamber (ThermoFisher, A7816) can also be used instead of MatTek imaging dishes. For single molecule imaging wash the 25 mm circular cover glasses in isopropanol, then plasma clean and store the cover glasses in isopropanol at 4 °C until use. They can be stored for >6 months at 4 °C.
3. It is essential to use medium without phenol red for fluorescence imaging to avoid excessive background fluorescence.
4. Janelia Fluor dyes can be inquired about at dyes.janelia.org or purchased from Promega.
5. One can minimize localization uncertainty by choosing the objective magnification and camera pixel size such that the pixel size approximately matches the PSF standard deviation [37].
6. Our Matlab version of the MTT algorithm can be accessed here https://gitlab.com/tjian-darzacq-lab/SPT_LocAndTrack.
7. The web-interface can be found at https://spoton.berkeley.edu/SPTGUI/; the Matlab version at https://gitlab.com/tjian-darzacq-lab/spot-on-matlab; and the Python version at https://gitlab.com/tjian-darzacq-lab/Spot-On-cli.
8. If extra Matrigel dishes are coated, they can be sealed with Parafilm and stored in 4 °C for 2–4 days. It is recommended to prepare imaging dishes with Matrigel fresh.
9. Pipet up and down ~10–15 times until cells are dissociated into a single cell suspension. Check under a light microscope to ensure that they are in a single-cell suspension. If mESCs are passaged in clumps, they may differentiate.
10. Optimization of the dye concentration is typically required. For optimizing SPT experiments, we recommend a dye titration experiment using logarithmically spaced concentrations. Labeling will depend on protein concentration, cell type, incubation time, and must thus be optimized for each cell line. For regular Halo-JF dyes, we typically use between ~1 pM and ~5 nM labeling. For photoactivatable Halo-JF dyes, we typically use ~5 nM to ~100 nM. For SPT, complete labeling is neither necessary nor desired. But if complete labeling is desired, 500 nM JF-Halo dye is typically sufficient as shown in [54].
11. When using "regular" JF-HaloTag dyes, two short 5-min washes are generally sufficient. However, for PA-JF dyes, more washes and/or longer than 5-min washes may be required. The optimal washing protocol can be both dye and cell-type specific. As a control, we recommend labeling and washing a wild-type cell that does not express HaloTag and making sure that negligible dye remains in this negative control.

12. Click on "learn more" to see the details of the format. If your trajectory format is not identical to any of the supported format, it will be necessary to first write a script to convert it to one of the Spot-On supported formats. Sample files for each support format are available.
13. More data is always better, but we recommend having at least 6 single cells per condition and at least a few thousand trajectories with at least 3 detections (*see* Fig. 3—figure supplement 12 in [28] for a quantification of how the robustness of the Spot-On fit depends on the number of trajectories). It is also worth paying close attention to "Particles per frame"—if this number is too high, the SPT data is likely to contain frequent tracking misconnections.
14. For a full discussion of how to choose these parameters, please *see* Appendix 2 in [28] and the documentation available at https://spoton.berkeley.edu/SPTGUI/docs/latest. Here, we provide brief guidance:

    Bin width: Bin width used to make displacement histograms and used for PDF-fitting. Default is 10 nm and is generally reasonable unless you have very sparse data. 1 nm is the default setting for CDF-fitting, since CDF-fitting is more robust and less prone to binning artifacts.

    Number of timepoints: How many timepoints to consider in the displacement histogram. If you allow $N$ time points, this corresponds to considering displacements with a maximal time-delay of up to $(N-1)\Delta t$. Generally, displacement histograms become sparser at large time-delays and we generally do not recommend considering time-delays much above 50–60 ms.

    Max jump: the maximal displacements that will be considered in the analysis. This should be larger than the largest displacements in the data. Generally, 3–5 μm is reasonable.

    Jumps to Consider and "Use entire trajectories": If use entire trajectories is set to Yes, all displacement data will be used. If it is set to No, only up to the indicated value of Jumps to consider is used. For example, if Jumps to consider is set to 4 and 8 timepoints, for each trajectory, 4 displacements (if possible) will be used to compute the displacement histogram such that a trajectory of nine frames will contribute four displacements to $1\Delta t$, four displacements to $2\Delta t$, . . ., and two displacements to $7\Delta t$. This is a semiempirical way of correcting for additional biases toward bound molecules, and if there is no bias toward bound molecules in the raw data, "Use entire trajectories" should be set to Yes. This is a subtle choice and please *see* Appendix 2 referenced above for a more complete discussion.

15. As noted above, please *see* Appendix 2 in [28] and the documentation available at https://spoton.berkeley.edu/SPTGUI/docs/latest for a full discussion. It is described briefly below.

    Kinetic model: this choice is discussed in the main text. We recommend starting with the two-state model, and only considering the three-state model if the two-state fit is quite poor and/or there are biochemical and mechanistic reasons to suspect two distinct freely diffusive states.

    Upper and lower bounds on fitted diffusion coefficients: Defaults are [0.0005–0.08 $\mu m^2/s$] for $D_{BOUND}$ and [0.15–0.25 $\mu m^2/s$] for $D_{FREE}$. Please *see* Appendix 2 in [28] for a full discussion, but briefly, it is important to pay attention to these and make sure Spot-On does not infer a $D$ at the min or max. Also, $D_{BOUND} = 0.08\ \mu m^2/s$ is almost certainly too high for DNA binding and could indicate that the specified localization error is too small and/or problems with microscope stability. It is very useful to perform SPT on a histone control to assess what $D_{BOUND}$ to expect from the bound population.

    Localization Error: this is the 1D standard deviation of the localization uncertainty. If this can be estimated independently and specified, it will improve the robustness of the fit. If it is fitted from the data, please note that it is mainly fitted from the bound subpopulation and that it is not well-fitted if the bound subpopulation is negligible. If the localization error is incorrectly specified, typically the fit to the bound subpopulation will be poor.

    $Z$ correction and d$Z$: since SPT generally involves 2D imaging of 3D motion, we must correct for defocalization. On most SPT microscopes, the axial detection range is ~700 nm—if particles move out of this range, they generally cannot be detected. Using ~700 nm is generally safe, but please *see* [28] for advice on how to experimentally measure it. In some organisms such as some yeasts and bacteria, the cell is so small, that the observation slice is comparable to the axial detection range, in which case the $Z$ correction should be set to "No," since there is no defocalization.

    Model fit: You can either fit the PDF or CDF of the displacement histogram. Generally, CDF-fitting is more robust since it is less susceptible to binning noise, especially for moderately sparse datasets. However, the two approaches give equivalent results for sufficiently large SPT datasets, and comparing PDFs and fits is generally more intuitive.

    Perform single cell fit: We generally recommend fitting each single cell and assessing each single cell fit. This can be a great way of identifying potentially problematic single cell movies and for assessing cell-to-cell variation. The only downside is that it will take significantly longer for Spot-On to run.

Iterations: Spot-On uses least-squares fitting, which is subject to trapping in local minima during optimization. For each fit iteration Spot-On will generate a random initial guess for each fitted parameter and proceed with optimization for a hard-coded number of steps or until convergence. To avoid trapping in local minima, multiple iterations of this are repeated. For the 2-state model, three iterations are typically more than enough to ensure that the global minima is identified. For 3-state model fitting, or if the fit looks poor, it may be worth increasing the number of fit iterations. The only downside to increasing the number of iterations is a slower fit.

16. Problematic dataset refers to potential outliers in the overall experimental dataset. For example, if an unhealthy cell or a mitotic cell was accidentally chosen, or if the particle density was too high, or is the acquisition settings were chosen poorly (improper TIRF angle, etc.). Looking at each single cell as well as the overall population can be a great way to assess cell-to-cell variation and to assess the robustness of conclusions.
17. BIC and AIC are information criteria that can be used to compare the "goodness of fit" for different models, while penalizing models with more parameters. However, since Spot-On models protein diffusion as Brownian, which it never truly is in cells, we note that using BIC or AIC to compare the goodness of fit of the 2-state and 3-state models can be misleading.

## Acknowledgments

We thank Domenic Narducci, Miles Huseyin, Jin Yang, Hugo Brandão, Viraat Goel, Sarah Nemsick, Shdema Filler-Hayut, Michele Gabriele, Jyothi Mahadevan, Meagan Esbin, Maxime Woringer, and Thomas Graham for insightful comments on the manuscript. We would like to acknowledge Davide Mazza, whose 2012 paper introduced the kinetic modeling framework that was ultimately implemented in Spot-On in a modified form, Maxime Woringer who codeveloped Spot-On and led the development of the web-interface and the Python version and who has been maintaining the web-interface, the Tjian-Darzacq lab for discussions during the development of Spot-On and for hosting the web-interface, and Luke Lavis for the development and sharing of Janelia Fluor dyes. We thank Domenic Narducci for the code to simulate the concept of motion-blurring in Fig. 5. This work was supported by the National Institutes of Health under grant numbers R00GM130896, DP2GM140938, and UM1HG011536.

## References


1. Lionnet T, Wu C (2021) Single-molecule tracking of transcription protein dynamics in living cells: seeing is believing, but what are we seeing? Curr Opin Genet Dev 67:94–102
2. Cramer P (2019) Organization and regulation of gene transcription. Nature 573:45–54
3. Phair RD, Misteli T (2000) High mobility of proteins in the mammalian cell nucleus. Nature 404:604–609
4. McNally JG, Müller WG, Walker D, Wolford R, Hager GL (2000) The Glucocorticoid Receptor: Rapid Exchange with Regulatory Sites in Living Cells. Science 287: 1262–1265. https://doi.org/10.1126/science.287.5456.1262
5. Mueller F, Stasevich TJ, Mazza D, McNally JG (2013) Quantifying transcription factor kinetics: at work or at play? Crit Rev Biochem Mol Biol 48:492–514
6. Mueller F, Mazza D, Stasevich TJ, McNally JG (2010) FRAP and kinetic modeling in the analysis of nuclear protein dynamics: what do we really know? Curr Opin Cell Biol 22:403–411
7. Politi AZ, Cai Y, Walther N, Hossain MJ, Koch B, Wachsmuth M, Ellenberg J (2018) Quantitative mapping of fluorescently tagged cellular proteins using FCS-calibrated four-dimensional imaging. Nat Protoc 13:1445–1464
8. Mazza D, Abernathy A, Golob N, Morisaki T, McNally JG (2012) A benchmark for chromatin binding measurements in live cells. Nucleic Acids Res 40:e119–e119
9. Shen H, Tauzin LJ, Baiyasi R, Wang W, Moringo N, Shuang B, Landes CF (2017) Single particle tracking: from theory to biophysical applications. Chem Rev 117:7331–7376
10. Goulian M, Simon SM (2000) Tracking single proteins within cells. Biophys J 79:2188–2198
11. Chen J, Zhang Z, Li L, Chen B-C, Revyakin A, Hajj B, Legant W, Dahan M, Lionnet T, Betzig E, Tjian R, Liu Z (2014) Single-molecule dynamics of enhanceosome assembly in embryonic stem cells. Cell 156:1274–1285
12. Garcia DA, Fettweis G, Presman DM, Paakinaho V, Jarzynski C, Upadhyaya A, Hager GL (2021) Power-law behavior of transcription factor dynamics at the single-molecule level implies a continuum affinity model. Nucleic Acids Res 49:6605. https://doi.org/10.1093/nar/gkab072
13. Reisser M, Hettich J, Kuhn T, Popp AP, Große-Berkenbusch A, Gebhardt JCM (2020) Inferring quantity and qualities of superimposed reaction rates from single molecule survival time distributions. Sci Rep 10: 1758
14. Hansen AS, Pustova I, Cattoglio C, Tjian R, Darzacq X (2017) CTCF and cohesin regulate chromatin loop stability with distinct dynamics. elife 6:e25776
15. Metzler R, Jeon J-H, Cherstvy AG, Barkai E (2014) Anomalous diffusion models and their properties: non-stationarity, non-ergodicity, and ageing at the centenary of single particle tracking. Phys Chem Chem Phys 16:24128–24164
16. Hansen AS, Amitai A, Cattoglio C, Tjian R, Darzacq X (2019) Guided nuclear exploration increases CTCF target search efficiency. Nat Chem Biol 16:257. https://doi.org/10.1038/s41589-019-0422-3
17. Loffreda A, Jacchetti E, Antunes S, Rainone P, Daniele T, Morisaki T, Bianchi ME, Tacchetti C, Mazza D (2017) Live-cell p53 single-molecule binding is modulated by C-terminal acetylation and correlates with transcriptional activity. Nat Commun 8:313
18. Popp AP, Hettich J, Gebhardt JCM (2021) Altering transcription factor binding reveals comprehensive transcriptional kinetics of a basic gene. Nucleic Acids Research, 49(11), pp.6249–6266
19. Nguyen VQ, Ranjan A, Liu S, Tang X, Ling YH, Wisniewski J, Mizuguchi G, Li KY, Jou V, Zheng Q, Lavis LD, Lionnet T, Wu C (2020) Spatio-Temporal Coordination of Transcription Preinitation Complex Assembly in live Cells. bioRxiv. https://doi.org/10.1101/2020.12.30.424853
20. Jain S, Shukla S, Yang C, Zhang M, Fatma Z, Lingamaneni M, Abesteh S, Lane ST, Xiong X, Wang Y, Schroeder CM, Selvin PR, Zhao H (2021) TALEN outperforms Cas9 in editing heterochromatin target sites. Nat Commun 12:606
21. Huseyin MK, Klose RJ (2021) Live-cell single particle tracking of PRC1 reveals a highly dynamic system with low target site occupancy. Nat Commun 12:887
22. Tatavosian R, Duc HN, Huynh TN, Fang D, Schmitt B, Shi X, Deng Y, Phiel C, Yao T, Zhang Z, Wang H, Ren X (2018) Live-cell single-molecule dynamics of PcG proteins imposed by the DIPG H3.3K27M mutation. Nat Commun 9:2080
23. Teves SS, An L, Hansen AS, Xie L, Darzacq X, Tjian R (2016) A dynamic mode of mitotic

bookmarking by transcription factors. elife 5: e22280

24. Deluz C, Friman ET, Strebinger D, Benke A, Raccaud M, Callegari A, Leleu M, Manley S, Suter DM (2016) A role for mitotic bookmarking of SOX2 in pluripotency and differentiation. Genes Dev 30:2538. http://genesdev.cshlp.org/content/early/2016/12/05/gad.289256.116.abstract
25. Chong S, Dugast-Darzacq C, Liu Z, Dong P, Dailey GM, Cattoglio C, Heckert A, Banala S, Lavis L, Darzacq X, Tjian R (2018) Imaging dynamic and selective low-complexity domain interactions that control gene transcription. Science 361:eaar2555
26. M. Mir, A. Reimer, M. Stadler, A. Tangara, A. S. Hansen, D. Hockemeyer, M. B. Eisen, H. Garcia, X. Darzacq, Y. L. Lyubchenko, Springer New York, NY, 2018; Single Molecule Imaging in Live Embryos Using Lattice Light-Sheet Microscopy. https://doi.org/10.1007/978-1-4939-8591-3_32, pp. 541–559
27. Manley S, Gillette JM, Patterson GH, Shroff H, Hess HF, Betzig E, Lippincott-Schwartz J (2008) High-density mapping of single-molecule trajectories with photoactivated localization microscopy. Nat Methods 5: 155–157
28. Hansen AS, Woringer M, Grimm JB, Lavis LD, Tjian R, Darzacq X (2018) Robust model-based analysis of single-particle tracking experiments with Spot-On. elife 7:e33125
29. Watanabe N, Mitchison TJ (2002) Single-Molecule Speckle Analysis of Actin Filament Turnover in Lamellipodia. Science 295:1083–1086. https://doi.org/10.1126/science.1067470
30. Gebhardt JCM, Suter DM, Roy R, Zhao ZW, Chapman AR, Basu S, Maniatis T, Xie XS (2013) Single-molecule imaging of transcription factor binding to DNA in live mammalian cells. Nat Methods 10:421
31. Presman DM, Ball DA, Paakinaho V, Grimm JB, Lavis LD, Karpova TS, Hager GL (2017) Quantifying transcription factor binding dynamics at the single-molecule level in live cells. Methods 123:76–88
32. Shao S, Xue B, Sun Y (2018) Intranucleus single-molecule imaging in living cells. Biophys J 115:181–189
33. Los GV, Encell LP, McDougall MG, Hartzell DD, Karassina N, Zimprich C, Wood MG, Learish R, Ohana RF, Urh M, Simpson D, Mendez J, Zimmerman K, Otto P, Vidugiris G, Zhu J, Darzins A, Klaubert DH, Bulleit RF, Wood KV (2008) HaloTag: a novel protein labeling technology for cell imaging and protein analysis. ACS Chem Biol 3:373–382
34. Grimm JB, English BP, Chen J, Slaughter JP, Zhang Z, Revyakin A, Patel R, Macklin JJ, Normanno D, Singer RH, Lionnet T, Lavis LD (2015) A general method to improve fluorophores for live-cell and single-molecule microscopy. Nat Methods 12:244
35. Grimm JB, English BP, Choi H, Muthusamy AK, Mehl BP, Dong P, Brown TA, Lippincott-Schwartz J, Liu Z, Lionnet T, Lavis LD (2016) Bright photoactivatable fluorophores for single-molecule imaging. Nat Methods 13:985
36. Tokunaga M, Imamoto N, Sakata-Sogawa K (2008) Highly inclined thin illumination enables clear single-molecule imaging in cells. Nat Methods 5:159–161
37. Thompson RE, Larson DR, Webb WW (2002) Precise nanometer localization analysis for individual fluorescent probes. Biophys J 82:2775–2783
38. Elf J, Li G-W, Xie XS (2007) Probing Transcription Factor Dynamics at the Single-Molecule Level in a LivingCell. Science 316: 1191–1194. https://doi.org/10.1126/science.1141967
39. Izeddin I, Récamier V, Bosanac L, Cissé II, Boudarene L, Dugast-Darzacq C, Proux F, Bénichou O, Voituriez R, Bensaude O, Dahan M, Darzacq X (2014) Single-molecule tracking in live cells reveals distinct target-search strategies of transcription factors in the nucleus. elife 3:e02230
40. Chenouard N, Smal I, de Chaumont F, Maška M, Sbalzarini IF, Gong Y, Cardinale J, Carthel C, Coraluppi S, Winter M, Cohen AR, Godinez WJ, Rohr K, Kalaidzidis Y, Liang L, Duncan J, Shen H, Xu Y, Magnusson KEG, Jaldén J, Blau HM, Paul-Gilloteaux P, Roudot P, Kervrann C, Waharte F, Tinevez J-Y, Shorte SL, Willemse J, Celler K, van Wezel GP, Dan H-W, Tsai Y-S, de Solórzano CO, Olivo-Marin J-C, Meijering E (2014) Objective comparison of particle tracking methods. Nat Methods 11:281–289
41. Deschout H, Neyts K, Braeckmans K (2012) The influence of movement on the localization precision of sub-resolution particles in fluorescence microscopy. J Biophotonics 5:97–109
42. Lee A, Tsekouras K, Calderon C, Bustamante C, Pressé S (2017) Unraveling the thousand word picture: an introduction to super-resolution data analysis. Chem Rev 117: 7276–7330
43. Tinevez J-Y, Perry N, Schindelin J, Hoopes GM, Reynolds GD, Laplantine E, Bednarek SY, Shorte SL, Eliceiri KW (2017) TrackMate:

an open and extensible platform for single-particle tracking. Methods 115:80–90

44. Sergé A, Bertaux N, Rigneault H, Marguet D (2008) Dynamic multiple-target tracing to probe spatiotemporal cartography of cell membranes. Nat Methods 5:687–694
45. Jaqaman K, Loerke D, Mettlen M, Kuwata H, Grinstein S, Schmid SL, Danuser G (2008) Robust single-particle tracking in live-cell time-lapse sequences. Nat Methods 5:695–702
46. Shivanandan A, Radenovic A, Sbalzarini IF (2013) MosaicIA: an ImageJ/Fiji plugin for spatial pattern and interaction analysis. BMC Bioinformatics 14:349
47. Persson F, Lindén M, Unoson C, Elf J (2013) Extracting intracellular diffusive states and transition rates from single-molecule tracking data. Nat Methods 10:265
48. Monnier N, Barry Z, Park HY, Su K-C, Katz Z, English BP, Dey A, Pan K, Cheeseman IM, Singer RH, Bathe M (2015) Inferring transient particle transport dynamics in live cells. Nat Methods 12:838–840
49. Vink JNA, Brouns SJJ, Hohlbein J (2020) Extracting transition rates in particle tracking using analytical diffusion distribution analysis. Biophys J 119:1970–1983
50. Karslake JD, Donarski ED, Shelby SA, Demey LM, DiRita VJ, Veatch SL, Biteen JS (2020) SMAUG: analyzing single-molecule tracks with nonparametric Bayesian statistics. Methods 193:16. https://doi.org/10.1016/j.ymeth.2020.03.008
51. Kues T, Kubitscheck U (2002) Single molecule motion perpendicular to the focal plane of a microscope: application to splicing factor dynamics within the cell nucleus. Single Mol 3:218–224
52. Lu H, Yu D, Hansen AS, Ganguly S, Liu R, Heckert A, Darzacq X, Zhou Q (2018) Phase-separation mechanism for C-terminal hyperphosphorylation of RNA polymerase II. Nature 558:318–323
53. Mangel WF, McGrath WJ, Xiong K, Graziano V, Blainey PC (2016) Molecular sled is an eleven-amino acid vehicle facilitating biochemical interactions via sliding components along DNA. Nat Commun 7:10202
54. Cattoglio C, Pustova I, Walther N, Ho JJ, Hantsche-Grininger M, Inouye CJ, Hossain MJ, Dailey GM, Ellenberg J, Darzacq X, Tjian R, Hansen AS (2019) Determining cellular CTCF and cohesin abundances to constrain 3D genome models. elife 8:e40164